Polymer 296 (2024) 126816

Contents lists available at ScienceDirect

Polymer

journal homepage: www.elsevier.com/locate/polymer

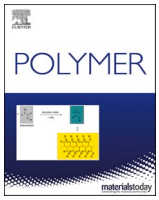

Isothermal crystallization of poly(vinylidene fluoride) blended with the ionic liquid $[Emim]_2[Co(SCN)_4]$: Simultaneous analysis of crystalline phases by infrared spectroscopy and differential scanning calorimetry

Luis A. Martins [a], José Luis Gómez Ribelles [a,b], Carlos M. Costa [c,d,*], Daniela M. Correia [e], Senentxu Lanceros-Méndez [c,d,f,g], Ivan Krakowsky [h], Isabel Tort-Ausina [a,b,**]

[a] Centre for Biomaterials and Tissue Engineering, CBIT, Universitat Politècnica de València, C/Camino de Vera S/n, 46022, Valencia, Spain
[b] CIBER de Bioingeniería, Biomateriales y Nanomedicina, Instituto de Salud Carlos III, Spain
[c] Physics Centre of Minho and Porto Universities, University of Minho, 4710-057, Braga, Portugal
[d] Laboratory of Physics for Materials and Emergent Technologies, LapMET, University of Minho, 4710-057, Braga, Portugal
[e] Centre of Chemistry, University of Minho, 4710-057, Braga, Portugal
[f] BCMaterials, Basque Center for Materials, Applications and Nanostructures, UPV/EHU Science Park, 48940, Leioa, Spain
[g] Ikerbasque, Basque Foundation for Science, 48009, Bilbao, Spain
[h] Department of Macromolecular Physics, Charles University 180 00 Prague 8, Czech Republic

ARTICLE INFO

Keywords:
PVDF
$[Emim]_2[Co(SCN)_4]$
Crystalline phases
DSC
FTIR
Crystallization kinetics

ABSTRACT

The combination of poly (vinylidene fluoride) (PVDF) with ionic liquids (ILs) is increasingly being studied for the development of smart materials. Together with the functional response provided by the IL, its incorporation into PVDF allows to nucleate specific electroactive phases of the polymer, depending on the processing conditions. Thus, the isothermal crystallization of PVDF incorporating different contents of the magnetic ionic liquid bis(1-ethyl-3-methylimidazolium) tetrathiocyanatocobaltate ($[Emim]_2$ $[Co(SCN)_4]$) is reported in this work.

Morphological properties of the films were obtained by field emission scanning electronic microscopy (FESEM), and particularly, for the higher contents of IL, segregation was observed through artifacts present on the film surface. This fact has been further confirmed by energy-dispersive x-ray spectroscopy (EDX).

The growth of the crystalline phases of PVDF during isothermal crystallization at different temperatures has been analyzed by Fourier transform infrared (FTIR) spectroscopy. Although α, β and γ crystalline phases were present in all samples, their relative percentages varied greatly with the amount of IL present, demonstrating that $[Emim]_2$ $[Co(SCN)_4]$ is a strong inductor of the electroactive (EA) phases of PVDF.

By evaluating both FTIR and DSC data, this effect has been ascribed to the higher melting temperatures of the EA structures whose formation is favored at higher crystallization temperatures. The melting temperature (T_m) of the β phase is higher than that of the α phase, whereas T_m for the γ phase is higher than for α and β phases.

Thus, together with the specific functional properties provided by the IL, such as magnetic response and ionic conductivity, the addition of $[Emim]_2$ $[Co(SCN)_4]$ strongly influences PVDF's crystallization kinetics, proving to be a simple and very effective way to nucleate specific phases of PVDF, according also to the specific processing conditions.

1. Introduction

Smart materials are being applied in different fields of knowledge, ranging from biomedicine to sensors, actuators and energy storage. Independently of the specific application, the characterization in terms of physical-chemical and functional properties of the developed smart materials is an essential step to understand the success of the material to a specific application [1].

Among the different types of polymeric materials capable of responding to external stimuli with a suitable functional response, poly

* Corresponding author. Physics Centre of Minho and Porto Universities, University of Minho, 4710-057, Braga, Portugal.
** Corresponding author. Centre for Biomaterials and Tissue Engineering, CBIT, Universitat Politècnica de València, C/Camino de Vera s/n, 46022, Valencia, Spain.
E-mail addresses: cmscosta@fisica.uminho.pt (C.M. Costa), isatort@fis.upv.es (I. Tort-Ausina).

https://doi.org/10.1016/j.polymer.2024.126816
Received 25 November 2023; Received in revised form 2 February 2024; Accepted 17 February 2024
Available online 19 February 2024

(vinylidene fluoride) (PVDF) has been extensively studied for a wide range of applications [2]. The high interest in PVDF relies in its high chemical, thermal, mechanical and radiation stability, as well as in its interesting piezo-, pyro- and ferroelectric properties. PVDF can crystallize in five distinct polymorphs, α, β, γ, ε and δ with the polymorph β exhibiting the highest piezoelectric response [3–5]. Further, PVDF presents good mechanical properties, flame retardancy, abrasion resistance and resistance to varying weather conditions [6].

PVDF has been combined with distinct fillers, aiming the development of smart materials to be applied in different fields, by tuning specific functional responses (e.g. dielectric or piezoelectric) or by providing novel ones (e.g. magnetic). This fillers include cobalt ferrite ($CoFe_2O_4$) [7–9], iron oxide (Fe_3O_4) [10,11], or lead zirconate titanate (PZT) particles [12,13], among others. Alternatively, the inclusion of salts composed entirely by cations and anions, denominated ionic liquids (ILs), represents a recent approach in the development of novel smart and functional materials [14]. ILs are receiving increasing attention for several fields of knowledge due to their ability to develop materials following green chemistry approaches, avoiding the toxicity associated with some solvents and particles used as fillers of polymeric matrices. Further, it is possible to develop ILs with varying functional properties through different combinations of organic cations and inorganic anions, allowing the development of ILs with thermochromic, magnetic, or highly ionic conductive characteristics, among others [14,15]. ILs also present high chemical stability, low volatility, negligible vapor pressure and a wide electrochemical window [16–18].

The interesting properties of ILs have led to their incorporation into different polymer matrices, being processed also into different morphologies depending on the intended application. In this context and due to the interesting PVDF and ILs properties, PVDF/IL composites have been obtained by using 1-butyl-3-methylimidazolium hexafluorophosphate ([BMIM][PF_6]), for improving water flux [19] 1-ethyl-3-methylimidazolium bis(trifluoromethylsulfonyl)imide ([EMIM][TFSI]), for improve the ionic conductivity [20], or IL-composites for application in sensors/actuators and energy storage devices [14], among others.

Based on the strong IL potential to be applied in different fields of knowledge, some relevant issues concerning the IL effect on PVDF physical-chemical properties as a result of the interactions between the IL and the polymer chain must be addressed. Studies reported that independently of the IL type, its inclusion into PVDF modifies its crystallization, inducing crystallization into β or, at higher temperatures, the γ phase [21].

The monitorization of the crystallization from the melt between 120 and 162 °C of semicrystalline PVDF/1-ethyl-3-methylimidazolium hexafluorophosphate [Emim][PF_6] blends revealed the formation of crystallites in both β and γ electroactive phases [21]. However, most of the studies on the influence of the IL on PVDF crystallization kinetics are performed during the cooling process from temperatures above the melting temperature of PVDF, whose results can be difficult to interpret using just a single experimental technique based on the multiple phases of the PVDF.

The crystallization of PVDF in the β phase in IL-PVDF blends has been studied for different ILs with the same cation 1-ethyl-3-methylimidazolium [Emim] and for ILs with the same anion bis(trifluoromethylsulfonyl)imide [TFSI] in which the cation [Emim] enhances the PVDF crystallization in the β-phase and the anion [TFSI] produces a mixture of α and β phases [22].

In this context, considering that imidazolium-based ILs are safe, nontoxic, low cost [23], and affect the crystallization process of PVDF, the goal of this work is to study for the first time the isothermal crystallization of PVDF in combination with the IL bis(1-ethyl-3-methylimidazolium) tetrathiocyanatocobaltate ([Emim]$_2$[$Co(SCN)_4$]), incorporating a magnetic anion and, therefore, providing magnetic and magneto ionic response to the hybrid material [24]. In fact, magnetic ILs are being intensively studied for combining the properties of ionic liquids with magnetism [25], and can provide, together with the electroactive properties of PVDF, a new class of highly multifunctional materials [14]. In this context, monitoring crystallization by infrared spectroscopy and differential scanning calorimetry at the same crystallization temperature makes it possible to reach conclusions about the formation of the electroactive phases at each crystallization temperature, relevant for the scientific understanding of the hybrid materials and for the proper determination of the processing conditions.

2. Experimental

2.1. Materials

All materials were used as received from the supplier. PVDF (6010) with a molecular weight between 300 000−330 000 Da was purchased from Solvay. The IL [Emim]$_2$ [$Co(SCN)_4$] (>99%) was purchased from Iolitec. N,Ndimethylformamide (DMF) (99.5% purity) was used as solvent and was purchased from Merck.

2.2. Sample preparation

Both PVDF and PVDF/[Emim]$_2$ [$Co(SCN)_4$] films were produced by a solvent casting method according to the procedure reported in Ref. [26]. First, PVDF was dissolved in DMF (15/85 % w/w: ratio polymer/-solvent). After the complete PVDF dissolution, the solution was spread onto a glass substrate and let to dry in an oven (P-Selecta) at 210 °C for 10 min, ensuring complete solvent removal [26]. A similar procedure was used for the processing of the PVDF/[Emim]$_2$ [$Co(SCN)_4$] films. In this case, different [Emim]$_2$ [$Co(SCN)_4$] contents (10, 20 and 40% w/w) were first dispersed in DMF. Then, PVDF was added and after its dissolution, a similar procedure to the one used to produce neat PVDF films was followed. The final thickness of the samples is ~50 μm.

2.3. Characterization techniques

Field Emission Scanning Electron Microscopy (FESEM) was performed on a Zeiss Ultra 55 at 2 kV using the in-lens type II secondary electrons detector. Samples were gold sputtered for 90 s under argon atmosphere in a Bal-Tek SCD005 system in order to increase the surface conductivity and enhance imaging resolution. Samples were treated in a DSC apparatus before FESEM observation in an attempt to eliminate some surface artifacts. After melting at 210 °C, temperature was dropped to 154, 150, 150 and 146 °C, for the 40, 20, 10 and 0% IL content samples, respectively, at 120 °C/min and isothermally crystallized for 20 min, and finally, samples were cooled to room temperature.

Energy dispersive X-Ray (EDX) analysis was performed in a Zeiss Ultra 55 FE-SEM microscope with an Oxford X-MaxN silicon drift detector attachment. Data collection was performed at 15 kV through the Aztec EDX analysis software from Oxford Instruments.

Fourier transform infrared spectroscopy (FTIR) spectra were obtained in the attenuated reflection mode using a Nicolet 6700 spectrometer equipped with deuterated triglycine sulfate (DTGS) detector, KBr beam splitter, and horizontal micro-ATR Golden Gate unit (SPECAC), with a diamond crystal, enabling isothermal ATR-FTIR measurements at selected temperatures. A small amount of sample was spread on the diamond crystal at room temperature using a spatula, heated to 200 °C and kept in molten state at 200 °C for 5 min. Then it was cooled down at 15 °C/min to the selected crystallization temperature. After achieving the required crystallization temperature, the ATR-FTIR spectra collection was started. Sixty-four scans with spectral resolution 4 cm^{-1} were coadded to achieve a good signal-to-noise ratio at each isothermal crystallization time.

FTIR spectra were also acquired using a Spectrum 100, PerkinElmer, in attenuated total reflection mode over a range of 4000 to 400 cm^{-1} with a resolution of 4 cm^{-1}. Those FTIR spectra were obtained from the

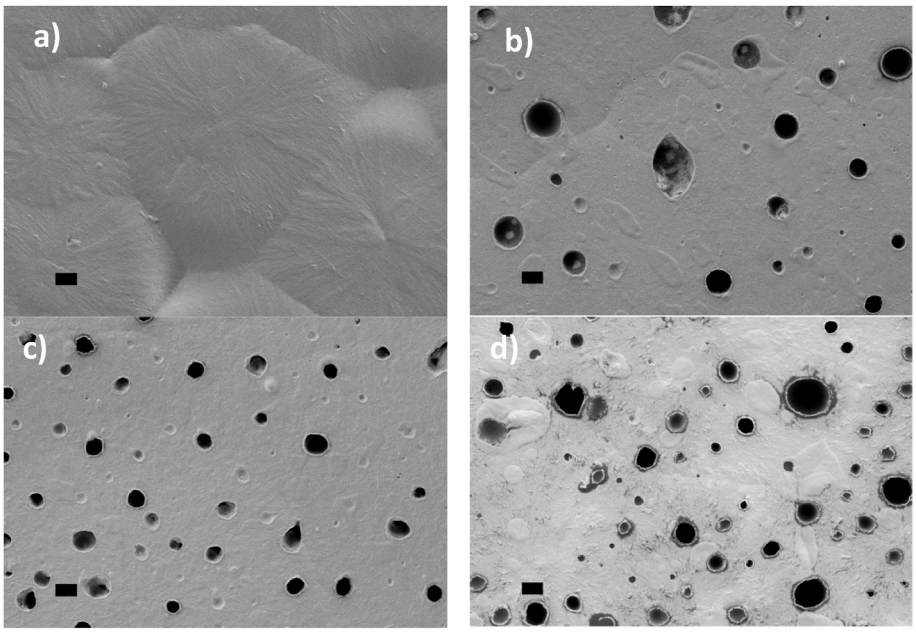

Fig. 1. FESEM images of PVDF films with different $[Emim]_2$ $[Co(SCN)_4]$ contents: a) 0 wt%, b) 10 wt%, c) 20 wt% and d) 40 wt%. Scale bar (bottom left in the images) 2 μm.

untreated PVDF and PVDF/$[Emim]_2$ $[Co(SCN)_4]$ samples, before the isothermal crystallization experiments were performed.

Differential scanning calorimetry (DSC) were carried out with a DSC 8000 from PerkinElmer to scan the crystallization and melting regions, in both cases under a flowing nitrogen (N_2) atmosphere of 20 ml/min. Samples were prepared with a mass between 2 and 6 mg. Cooling thermograms were recorded between 200 and 0 °C at 20 °C/min cooling rate, to determine the crystallization onset point. For isothermal crystallization experiments, samples were heated to 200 °C, kept at that temperature for 5 min, and then cooled down to the specific crystallization temperature at 90 °C/min, the highest cooling rate at which the DSC was kept under control during the whole cooling scan.

The Avrami equation can be applied to isothermal crystallization experiments [27–29]:

$$\frac{X_{ct}}{X_{c\infty(T)}} = 1 - exp(-kt^n) \tag{1}$$

And

$$\dot{q}(t) = X_{c\infty}(T)\frac{\rho_c}{\rho}\Delta H_f^0\frac{dX_c}{dt} \tag{2}$$

Where $X_{c\infty}$ is the maximum crystalline fraction, k is the overall crystallization rate constant, n is the Avrami exponent, $\dot{q}(t)$ is the DSC heat flow by the sample at time t, ρ and ρ_c are the density of the semi-crystalline PVDF and that of the crystal phase and ΔH_f^0 is the melting enthalpy.

2.4. Analytical methods

To calculate the electroactive (EA) phase fraction (sum of β and γ) of PVDF, Equation (2)was applied as follows [8,9,30,31]:

$$F(\mathrm{EA}) = \frac{A_{\mathrm{EA}}}{\left(\frac{K_{\mathrm{EA}}}{K_{\mathrm{a}}}\right)A_{\mathrm{a}} + A_{\mathrm{EA}}} \tag{2a}$$

In which the percentage of EA-phase is represented by F (EA), the deconvoluted peak areas at 766 and 840 cm^{-1} (corresponding to α and EA phases, respectively) are identified by A_a and A_{EA} and their corresponding absorption coefficients, namely $6.1x10^4$ and $7.7x10^4$ cm/mol, by K_a and K_{EA} [9,32].

To isolate the independent contributions of β and γ bands from the overall EA-phase, Equation (3) was applied as follows:

$$F(\gamma) = F(EA) \times \left(\frac{A_\gamma}{A_\gamma + A_\beta}\right) \times 100 \tag{3}$$

In which the percentage of γ-phase is represented by F(γ), the overall percentage of electroactive phase by F (EA) and the relative intensity absorbance at 1234 and 1275 cm^{-1} (corresponding to β and γ peaks, respectively) are represented by A_β and A_γ [33].

Equation (2) is based on ref [33] in which a method for the independent quantification of β and γ-phases through FTIR analysis is presented. The method was initially based on the differences between peak intensities at 1230 (γ) and 1275 cm^{-1} (β) and their closest valleys. Since PVDF and $[Emim]_2$ $[Co(SCN)_4]$ IR spectra overlap in the 1230 to 1275 cm^{-1} region, the method was adapted to perform the crystal phase calculation from the peak intensities isolated through IR spectra deconvolution.

3. Results and discussion

3.1. Morphological features

FESEM images of PVDF and PVDF/IL blend films evidence the morphological effects of the presence of $[Emim]_2$ $[Co(SCN)_4]$ within the polymer matrix, as shown in Fig. 1. Crystallites can be observed in all samples, although they are much more evident and clearer in Fig. 1a, representing the pristine PVDF sample, where there is no influence of the IL. Crystallites appear in the shape of polygonal areas, where a central nucleation point and the interfaces with neighboring crystallites can be also appreciated. Although a thermal fusion treatment was performed in an attempt to eliminate superficial artifacts from the processed samples, they were still observed, excluding the hypothesis that they could be originated by solvent escaping during processing. Fig. 1a differs greatly from Fig. 1b–d, where a series of stains and holes with diameters ranging between 0.5 and 4 μm are visible on the sample's surface. It is observed that the holes have variable depths; some of them

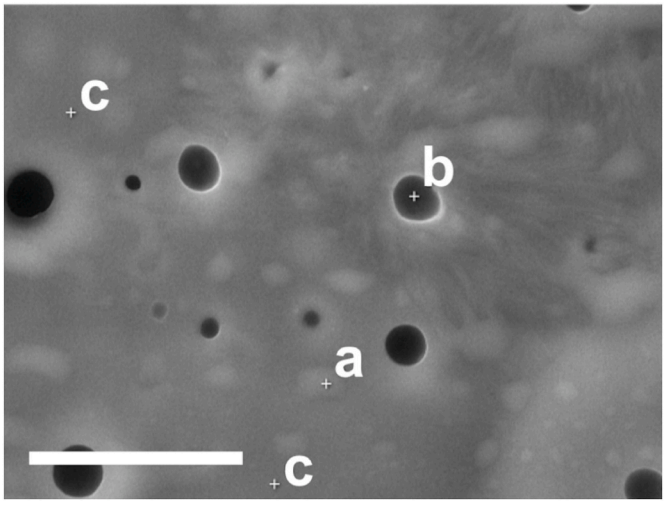

Fig. 2. FESEM images of 40 wt% $[Emim]_2$ $[Co(SCN)_4]$/PVDF film used for EDX analysis; white crosses mark the points of analysis for the different structures, a) stain, b) hole and c) polymer matrix. Scale bar 10 μm.

Table 1
Weight percentage of C, F, S and Co elements for the various structures observed at the surface of the 40 wt% $[Emim]_2$ $[Co(SCN)_4]$/PVDF sample. Average value and its standard deviation (SD) are shown.

	C Average (SD)	F Average (SD)	S Average (SD)	Co Average (SD)
bubble	64.14 (1.72)	21.63 (2.10)	9.44 (1.98)	4.78 (0.87)
hole	48.41 (9.90)	15.30 (3.04)	22.93 (9.40)	12.99 (4.16)
surface	70.90 (1.45)	19.96 (1.09)	6.56 (1.22)	2.58 (0.81)

are very shallow while others are seemingly deeper. These holes and stains are likely due to the presence of the IL escaping or getting close but not being able to burst the PVDF's top layer. Images for the 10 and 20 wt% samples (Fig. 1b and c) do not differ much among them, but when the IL amount reaches 40 wt% (Fig. 1d) the surface seems much more affected: holes and stains are larger, as a direct consequence of the higher IL content that is segregated, while the surface appears rougher and full of different spots that are not visible for lower IL concentrations, as a consequence of the higher interaction between the IL and PVDF.

Optical microscopy seems to indicate phase separation during crystallization. When melted, the sample exhibits a more homogeneous structure without visible artifacts. Upon cooling, white lines are observed, as shown in Fig. S1 (supplementary information). Optical imaging lacks the definition and magnification needed to observe the artifacts, which are show in the FESEM images of Fig. 1b, c and d, allowing to clarify the origin of the observed structures. On the other hand, the lack of observable structures and homogeneous aspect of the melted sample and the marked impact of the IL presence on the crystal type formed indicate a close contact between IL and PVDF. Therefore, all data seems to indicate admixing of both phases while in melted state with IL segregation occurring during the crystallization phase, hence crystallization from a homogeneous mixture.

This hypothesis is backed by the energy dispersive x-ray spectroscopy (EDX) data. Elemental analysis was performed on the different structures observed in the 40 wt% IL content samples surface, as indicated in Fig. 2 by the letter "a" situated in a stain, "b" in a hole and "c" in a zone of the polymer matrix, the latter analyzed in two different places. The evaluation was performed in three different samples, and the average of each structure elements was calculated, obtaining the data that are summarized in Table 1 and EDX spectra in supplementary information (Fig. S2).

All elements analyzed, whether common for polymer and IL (C), specific for PVDF (F) or specific for $[Emim]_2$ $[Co(SCN)_4]$ (S and Co), can be found for all analyzed regions, revealing their presence throughout the films, although their percentages varied regarding the type of structure: a) and b) structures show a lower C and F content and higher S and Co content when compared to c) structures, indicated a higher presence of IL at these regions. By comparing a) and b), IL specific elements appear in higher percentages in b) structures, supporting the hypothesis that b) structures have busted into the surface while a) structures did not, and are covered in a polymer layer. It is important to keep in mind that EDX was performed at a high beam intensity (15 kV), penetrating deeper than usual for FESEM imaging, and the signals detected come from a volume and not just from the surface.

The crystallization of PVDF starts from a molten mixture of PVDF and IL at 200 °C. The possibility of some liquid phase separation already at high temperature or during the abrupt cooling to the crystallization temperature cannot be ruled out, although it could not be observed experimentally. The marked effect of the presence and fraction of IL in the mixture on PVDF crystal nucleation suggests in any case that when crystallization is initiated there exist an interaction at molecular level between the IL molecules and the PVDF chain segments in the liquid phase. During PVDF crystallization, the PVDF crystals segregate from the liquid blend in the form of lamellae, thus highly increasing the ratio of IL to PVDF in the amorphous remaining regions. A part of the IL may end up mixed with the amorphous phase of PVDF, occupying the inter-lamellar space while another part is pushed into the inter-spherulite space or to the surface, as seen in other mixtures of PVDF and ILs [21, 22]. The shape observed in the FESEM images leads to think that a part of the IL remains close to the surface. In this regard, it should be mentioned that the thickness of the samples (~50 μm) is comparable to the size of the PVDF spherulites, as seen in Fig. 1a.

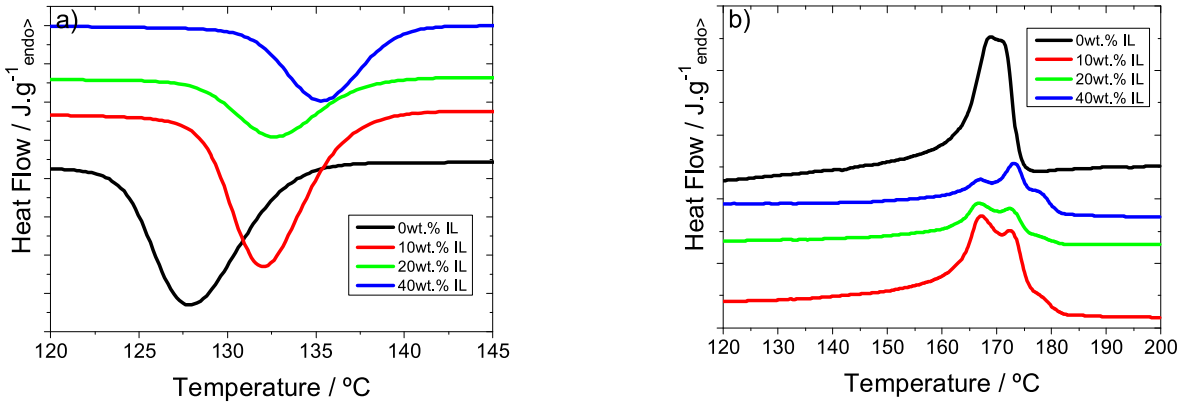

Fig. 3. a) Cooling DSC scans of PVDF/IL mixtures containing different percentages of IL and b) Heating scan measured after crystallization on the cooling ramp.

Table 2
Exothermal crystallization temperatures (T_{exo}), selected FTIR crystallization temperatures (T_c), and α, β and γ crystalline phase percentages formed after crystallization at different T_c on samples containing different amounts of IL $[Emim]_2$ $[Co(SCN)_4]$. Each percentage is followed by its absolute fraction, showed after the slash: percentage/absolute percentage.

IL (%)	0			10			20			40		
T_{exo} (°C)	128			132			132			136		
T_c (°C)	138	142	146	142	146	150	142	146	150	146	150	154
α (%)	76/24	75/23	75/25	52/21	29/12	41/16	26/8	21/7	18/6	16/6	16/7	16/8
β (%)	7/2	9/3	12/3	13/5	20/8	33/13	22/7	29/9	27/9	30/12	28/13	26/13
γ (%)	17/5	16/5	13/4	36/15	50/21	26/11	52/17	50/16	55/19	53/21	56/26	59/30

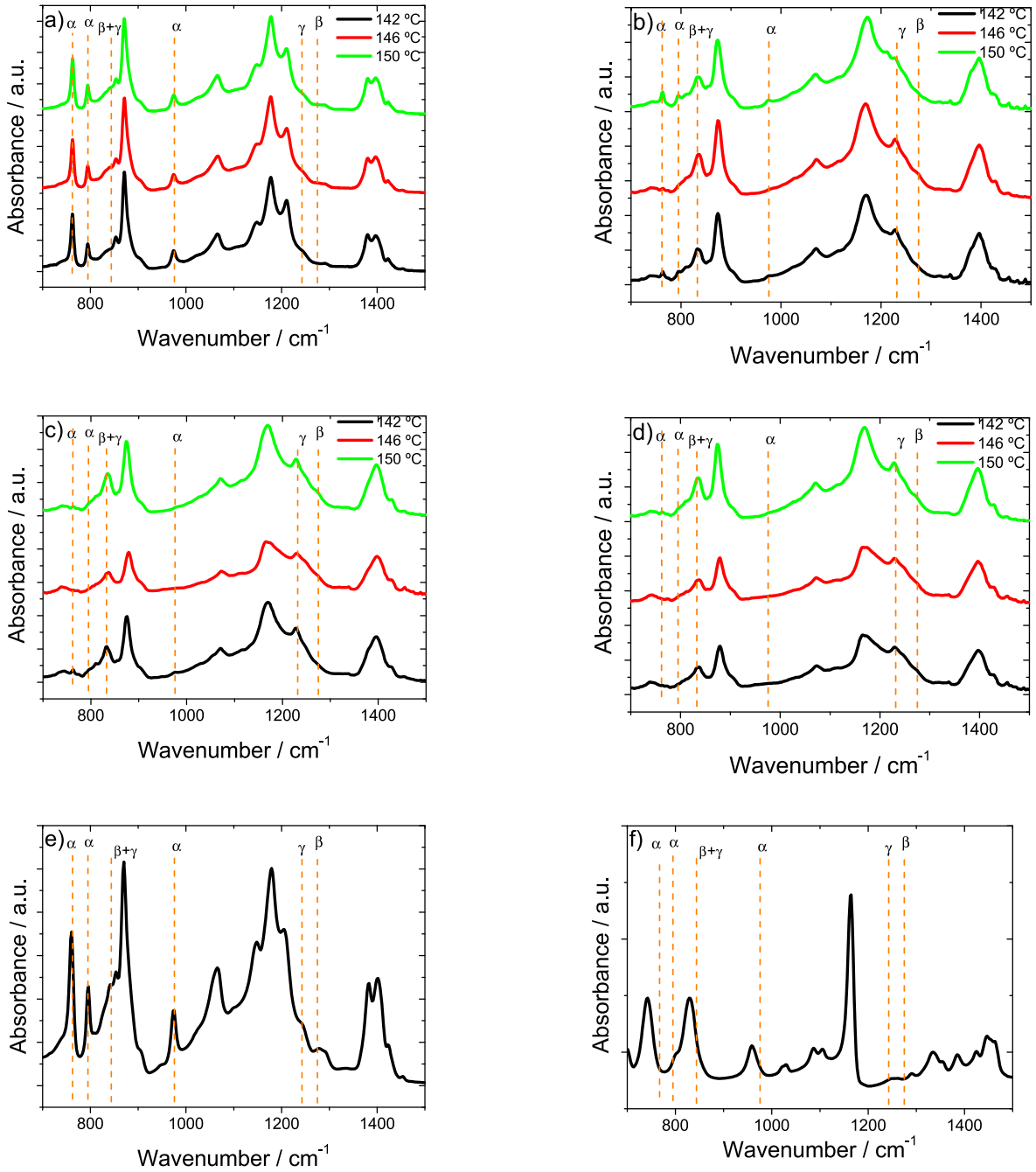

Fig. 4. FTIR absorbance spectra of pristine PVDF samples (a), mixture containing respectively 10 wt% (b), 20 wt% (c) and 40 wt% (d) $[Emim]_2$ $[Co(SCN)_4]$ content and unprocessed PVDF (e) and $[Emim]_2$ $[Co(SCN)_4]$ (f).

Table 3
PVDF crystalline phases and corresponding infrared specific peaks.

Crystalline structure	Characteristic peaks (cm^{-1})	Vibrational mode
α-phase	614	CF_2 Stretching
	763	CF_2 Stretching
	795	CH_2 Stretching
	975	CH Stretching
β-phase	1276	CF Stretching
γ-phase	840	CH_2 Stretching
	1234	CF_2 Stretching

3.2. Crystallization process and polymer phase content

The crystallization process of PVDF in the mixtures varies significantly with their composition due to the freezing point depression, as in the liquid sample at 200 °C, the IL acts as a solute of PVDF. The equilibrium melting temperature of a system consisting of a polymer mixed with a low molecular weight substance decreases as the concentration of solute increases due to the cryoscopic descent [34,35]. The crystallization temperature would follow a similar pattern but at lower temperatures, due to the undercooling necessary for the crystallization nuclei to be stable. The cooling thermograms (measured at 20 °C/min), nevertheless, follow the opposite trend (Fig. 3a): the temperature of the minimum of the exothermic peak in the cooling scan (T_{exo}), associated with the crystallization process, increases as the IL content of the sample increases. This behavior is explained by the fact that the phase in which PVDF crystallizes depends on the IL content of the mixture, as the fraction of the β and γ phases, which have higher melting temperatures than the α phase, increases with increasing IL content. When a DSC heating scan is recorded after crystallizing the sample during the cooling ramp, the superposition of up to three endothermic peaks can be observed (Fig. 3b), that can be due to the presence of different crystalline phases that form in different temperature intervals during cooling. This complex behavior is analyzed in the following by combining the information from FTIR spectra and DSC thermograms.

Moreover, Fig. 3 shows that it is not possible to compare the crystallization kinetics or the crystalline phases that are formed for the same crystallization temperature in mixtures with different IL contents, because this temperature in each mixture is at a different distance from the melting temperature (T_m).

In order to draw comparisons among the different samples, we will take as reference the exothermal crystallization temperature (T_{exo}) obtained by performing a temperature scan at a cooling rate of 20 °C/min (Fig. 3a).

For the FTIR isothermal analysis, three crystallization temperatures (T_c) were chosen per sample based on 10, 14 and 18 °C deviations above the corresponding sample's T_{exo}. The T_c and T_{exo} values are displayed in Table 2. Although it is generally accepted that the γ phase of the polymer is favored at high temperatures, in the pure PVDF sample, the percentage of γ phase is low, and it does not change considerably with the temperature. The γ phase is induced when the IL is added, but with the 10 wt% sample the observed behavior is not homogeneous, as the γ percentage does not increase with the temperature, which could be attributed to a more heterogeneous distribution of the IL. However, in the 20 and 40 wt% samples, this homogeneous behavior is observed: the higher the temperature, the higher γ phase percentage.

Fig. 4 shows the FTIR spectra of PVDF mixed with different weight percentages of the IL $[Emim]_2$ $[Co(SCN)_4]$, namely 0, 10, 20 and 40 wt% and crystallized at different temperatures. Crystallization time was long enough to ensure the maximum crystalline fraction at each temperature (as in the isothermal DSC scan it can be seen that heat flow was stabilized). PVDF crystalline phases were identified by the detection of phase-specific absorption peaks as shown in Table 3 [5,32,33].

In the pristine PVDF sample, the presence of absorption peaks at 763 and 795 cm^{-1} is clearly observed (Fig. 4a) [33], demonstrating that the polymer crystallizes mainly in α structures. Nonetheless, the absorbance peak at 840 cm^{-1} indicates the presence of electroactive β and/or γ structures [33]. Further deconvolution of FTIR spectra allows the isolation of specific β and γ absorbance peaks at 1230 and 1276 cm^{-1}, respectively, and consequently their independent quantification [5,33]. Although these structures were also identified, they represent a much reduced fraction of the overall crystalline structures. The presence of mainly α structures in PVDF films processed at high temperatures/from the melt was expected, as stated elsewhere [26,36].

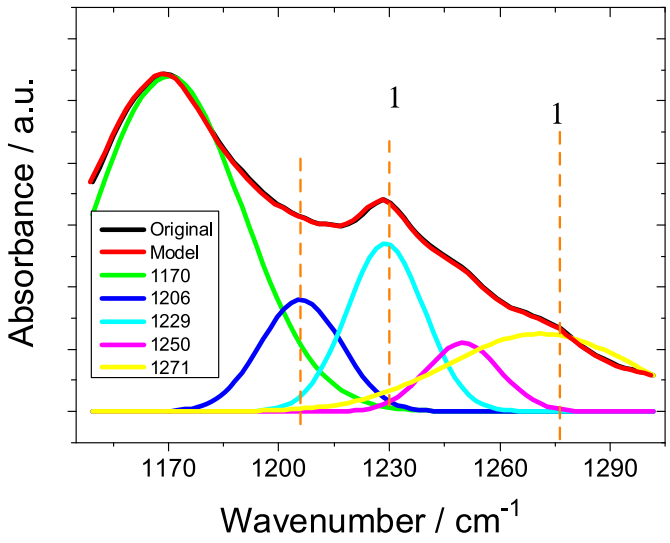

Fig. 5. FTIR spectrum deconvolution between 1140 and 1300 cm^{-1} for the PVDF/$[Emim]_2$ $[Co(SCN)_4]$ blend containing 20 wt% of IL crystallized at 150 °C.

In the samples containing different percentages of $[Emim]_2$ $[Co(SCN)_4]$, absorption peaks corresponding to all crystalline phases are observed, at 763, 795, 840, 975, 1230, and 1276 cm^{-1} (Fig. 4). When comparing pure PVDF (Fig. 4a) with the hybrid samples with mixtures of PVDF and IL (Fig. 4b, c and d), the relative intensities of the 763 and 795 cm^{-1} bands, corresponding to the α phase, are greatly reduced, while electroactive (γ+β), γ and β bands at 840, 1230 and 1276 cm^{-1}, respectively, are much more pronounced. Although all crystalline phases are present in all samples, their relative percentages varies greatly with the amount of IL, as presented in Table 2, demonstrating that $[Emim]_2$ $[Co(SCN)_4]$ is a strong inductor of the crystallization of PVDF in electroactive (EA) phases. Moreover, induction is dose-dependent, higher percentage of $[Emim]_2$ $[Co(SCN)_4]$ correlating with higher percentage of EA β and γ structures (as the reduction on the α phase is clearly shown in Table 2).

To quantify the various crystalline structures, the method developed by Martins et al. [8] was used, through the application of Equation (1) and Equation (2). Although, the superposition of $[Emim]_2$ $[Co(SCN)_4]$ and PVDF absorption peaks at the 765, 840, 1230 and 1276 cm^{-1} regions (Fig. 4e and f), leads to the need to perform further spectra deconvolution to isolate the intensity values of PVDF specific peaks for accurate crystal phase calculation (Fig. 5) [5,33].

The influence of the crystallization temperature on the percentage of each crystalline phase was also evaluated. Samples were crystallized at different temperatures (T_c values shown in Table 2) and their FTIR spectra were analyzed. Contrary to what happens when the percentage of IL varies, the effect of the T_c in the crystallization phase is very mild and it is not even observed in some cases. However, in some cases, crystallization at higher temperatures seems to promote reduced crystallization in α phase and increased crystallization in β and γ phases.

Table 2 shows the fractions of each crystalline phase in the different samples and for the different thermal treatments. Both the marked effect of the IL percentage and the mild, and sometimes negligible, effect of T_c on the relative percentages of crystalline phases are clearly observed.

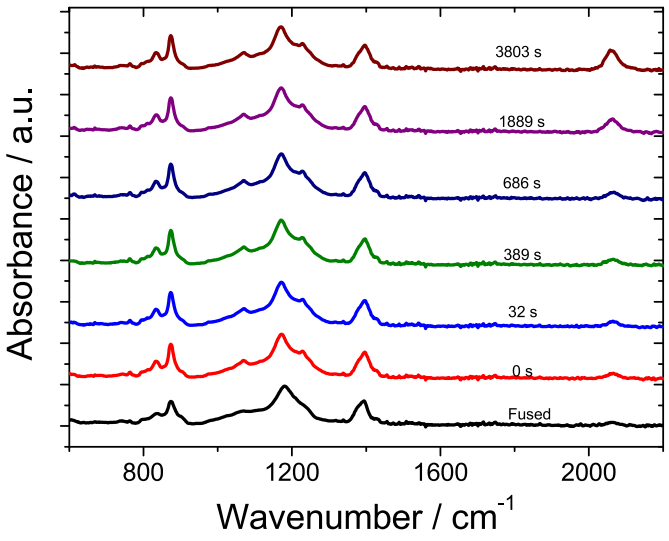

Fig. 6. FTIR absorbance spectra of the PVDF for different crystallization times.

The α phase drops from 76% to 16% and β and γ phases increase from 7% to 13%–30% and 59%, respectively, with the addition of 40% $[Emim]_2$ $[Co(SCN)_4]$, with respect to the pristine polymer.

FTIR spectra analysis at different timepoints allows to determine the absorbance peak and chemical bond evolution during the crystallization process. Fig. 6 shows the FTIR spectrum of a PVDF sample containing 20% of $[Emim]_2$ $[Co(SCN)_4]$ crystallized at 142 °C with crystallization times from 0 to 3803 s. It is observed that crystallization time influences both the relative peak intensity and its position.

The inclusion of $[Emim]_2$ $[Co(SCN)_4]$ has a strong effect in directing PVDF crystallization to EA phases. Even at the lowest concentration tested, the presence of the IL more than doubles the percentage of EA structures, the effect being stronger for samples with higher IL percentages. Crystallizing PVDF in EA structures is of major interest since these correlate to the piezoelectric and dielectric properties of the polymer, leading to a wide range of applications [37,38]. Commonly, some post-processing is needed so PVDF can exhibit its properties of interest [26], these are labor and time expensive. Alternatively, the addition of nanoparticles can also induce similar effects, however these possess the risk of leaching causing health and environmental concern [39–42]. The addition of $[Emim]_2$ $[Co(SCN)_4]$ is a simple and very effective way to maximize PVDF's electroactive properties and since it is in liquid state it can be easily removed when needed.

3.3. Isothermal crystallization and melting behavior

Thermal properties of the samples were studied by DSC calorimetric curves. A first scan was performed to determine the crystallization temperatures (T_{exo}), as shown in Fig. 3. Once T_{exo} has been determined, isothermal crystallization essays were carried out at temperatures between 128 and 160 °C, at 2 °C intervals. These started by melting the samples at 200 °C, followed by cooling at 90 °C/min until T_c was reached. Then, an isothermal stage was carried out, in which the exothermal peak was measured leaving time for the heat flow to reach baseline, and finally a heating scan (back to 200 °C) was performed at 20 °C/min.

Fig. 7a) shows the isothermal DSC thermograms of PVDF/$[Emim]_2$ $[Co(SCN)_4]$ blends containing 20 wt% of IL crystallized at different temperatures. It can be observed from Fig. 7a) that when the

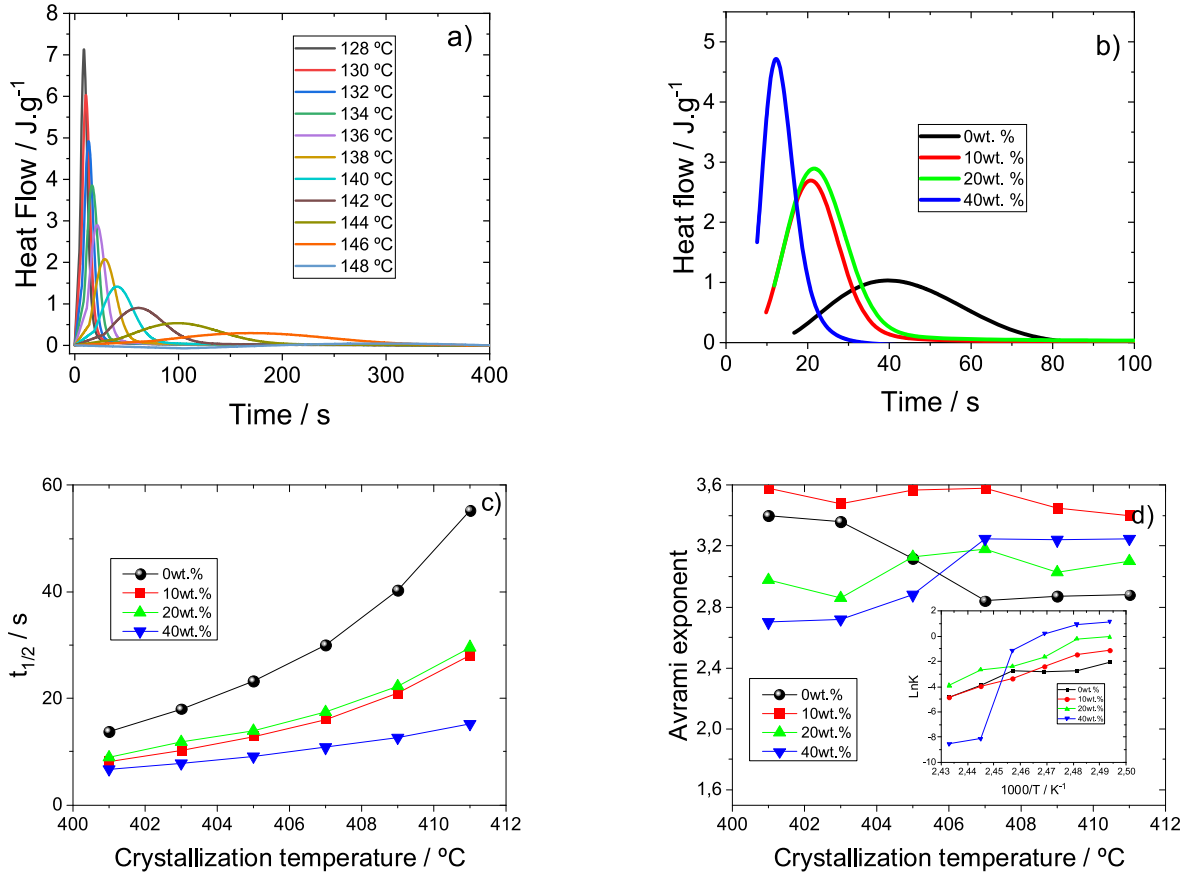

Fig. 7. a) Isothermal crystallization of the PVDF/$[Emim]_2$ $[Co(SCN)_4]$ blend containing 20 wt% of IL; b) DSC isotherms for the crystallization at 136 °C for all samples; c) $t_{1/2}$ and d) Avrami's exponent (n) as a function of crystallization temperature for all samples (insert: LnK vs Tc).

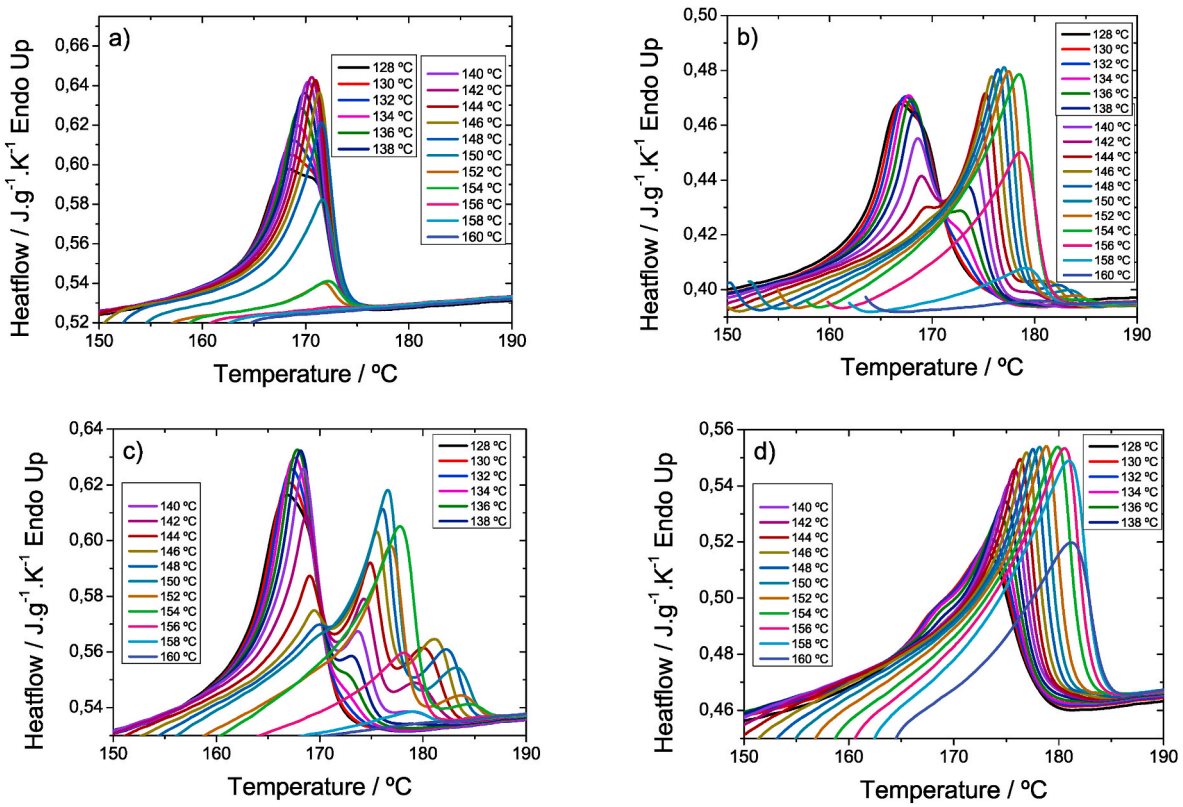

Fig. 8. DSC thermograms of neat PVDF (a) and mixtures with 10 wt% (b), 20 wt% (c) and 40 wt% (d) $[Emim]_2$ $[Co(SCN)_4]$ IL content, crystallized at different isothermal temperatures.

crystallization temperature (Tc) rises, the exothermic peak shifts to larger times and the peak width increases. This is because the rate of crystallization decreases as Tc increases. All samples also exhibit this property.

Fig. 7b) shows the DSC isotherms for the crystallization at 136 °C for all samples where it is detected that the peak corresponding to the maximum crystallization rate is much shifted toward lower times, demonstrating that the IL content accelerate the crystallization kinetics of PVDF what agrees with the results of the crystallization on cooling (Fig. 3a) that show the shift of the crystallization exotherm towards higher temperature as the IL content increases. This behavior is demonstrated through the half-time crystallization ($t_{1/2}$) as shown in Fig. 7c) for all crystallization temperatures. Fig. 7d) shows the Avrami exponent (n) and LnK as a function of crystallization for all samples. The Avrami exponent takes values around 3 in all the blends and crystallization temperatures. In pure PVDF it is observed to decrease slightly with the crystallization temperature while in the blends with 20 or 40 wt % IL the exponent n increases with Tc.

This value demonstrates spherical growth and homogeneous nucleation that depends on IL content, again due to the different crystalline phases that forms in the blends [43].

The heating scans performed after crystallization started at the same T_c, making sure the samples temperature never dropped below it. The thermograms of Fig. 8 show the melting behavior of the crystals formed during the isothermal stage.

In the neat PVDF, the melting process observed in the heating scan starts around 160 °C and its maximum appears at increasing temperatures as crystallization temperature T_c increases. This behavior was expected taking into account that as T_c increases, the thickness of the lamella that is formed during the crystallization also increases (Fig. 8a). According to the FTIR spectra, it can be stated that, to a large extent, this melting process corresponds to the melting of α phase crystals.

When PVDF is mixed with $[Emim]_2$ $[Co(SCN)_4]$, the IL acts as a solute of the PVDF. During the cooling scan, PVDF crystals have not been formed yet, as it is during the isothermal crystallization when neat PVDF crystals begin to form at the circle marked stage in Fig. 3. As a consequence, the IL fraction in the liquid phase increases. Once equilibrium is reached, the liquid phase in equilibrium with the PVDF crystals shall be a mixture of PVDF and IL.

The melting process in the subsequent heating scan starts from the crystallization temperature, the PVDF crystals start melting and are incorporated into the amorphous blend of PVDF and IL. In the DSC thermogram, the absorbed heat is due both to the melting heat of PVDF crystals and to the mixing heat of PVDF with the liquid phase. The melting process is then progressive, and the melting temperature (T_m) increases as the PVDF melts. This causes the shape of the endothermic peak to change in the blends containing 10 or 20 wt% of IL compared to neat PVDF. The process ends around the curve marking the dependence between melting temperature with solute concentration. Due to the freezing point depression, that temperature sits below the T_m of the neat PVDF crystals in the corresponding crystalline phase. In the thermograms corresponding to mixtures of 10 wt% and 20 wt% $[Emim]_2$ $[Co(SCN)_4]$ content, it is observed that the melting peaks corresponding to the α phase PVDF have shifted approximately 3 °C towards lower temperatures with respect to pristine PVDF. Thus, it can be defined an end set temperature for the melting peak by the intersection of the baseline with the tangent of the curve at the peak turning point, at the right of the maximum. It is observed that this temperature hardly depends on the T_c: it would be 174 °C in neat PVDF, 173 °C in the 10% mixture, and 171 °C in the 20% one.

Another important aspect is the undercooling required to begin crystallization. In neat PVDF, the melting peak area falls rapidly for T_c above 148 °C, and the melting peak is hardly observed at 154 °C. In 10% IL content mixtures, the peak height associated with the melting of the α phase begins to fall rapidly from T_c = 138 °C (Fig. 8b) and from T_c = 140 °C (Fig. 8c). In the 20 wt% IL content samples, this peak is

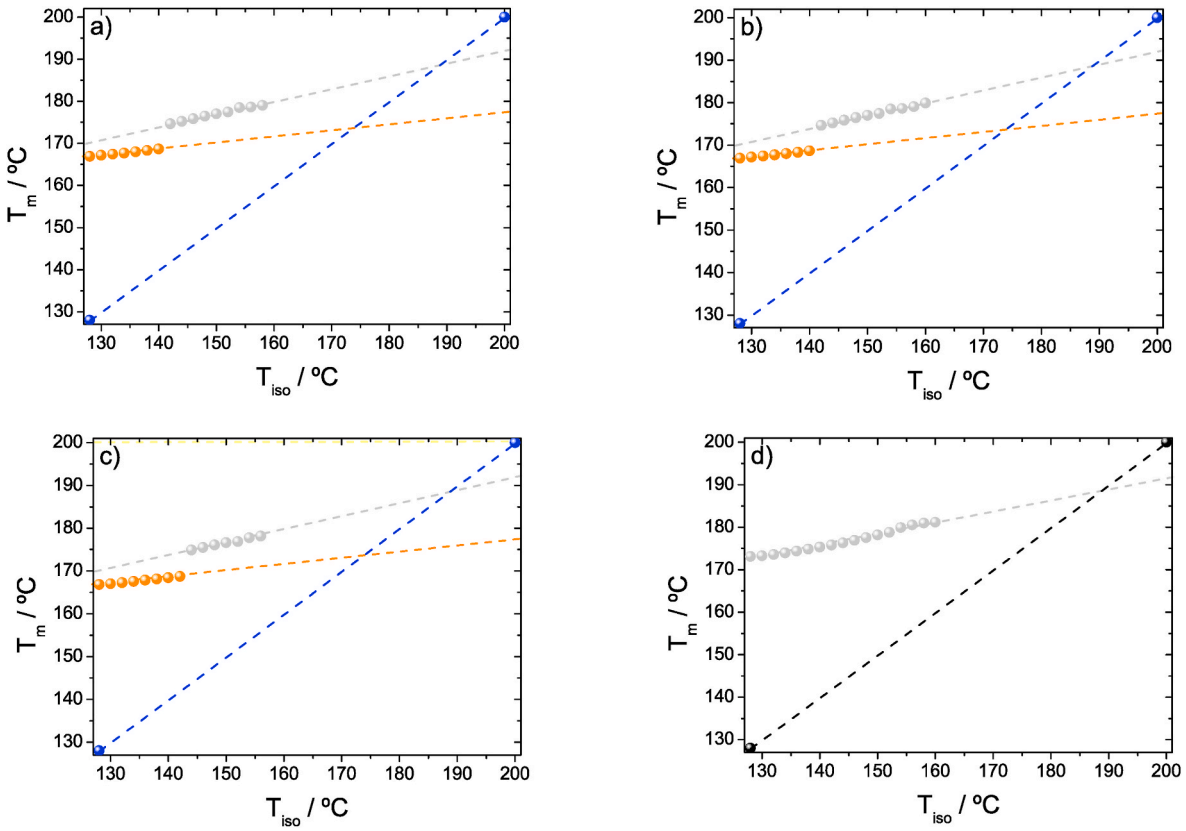

Fig. 9. Maximum melting temperature (T_m) as a function of the isothermal temperature (T_{iso}) of neat PVDF (a), and mixtures with 10 wt% (b), 20 wt% (c) and 40 wt % (d) $[Emim]_2$ $[Co(SCN)_4]$ IL content. The blue line is the $T_m = T_{iso}$ in all figures, orange points stand for α phase and grey points stand for β phase. (For interpretation of the references to colour in this figure legend, the reader is referred to the Web version of this article.)

practically negligible from 144 °C to 150 °C, respectively. In the 40 wt% IL content samples, melting in the temperature range in which neat α PVDF melts is still appreciable as a shoulder of the main endothermic peak, having the maximum at higher temperatures (Fig. 8d). Although in the DSC thermogram of the 40 wt% IL sample the α phase is not observed above 150 °C, it is appreciable in the FTIR spectrum. This could be due to the overlap with the β phase melting peak. Then, two more peaks are observed at higher T_m, which can be associated with the crystallization of PVDF in β and γ phases. It has been stated that the T_m of γ phase PVDF is higher than that of the α phase [44], whereas that of the β phase could be similar to the α-phase one. However, these results must be taken into consideration carefully since in these works the different phases have been obtained with different thermal histories, and T_m is highly dependent on T_c, as it has been shown previously.

In the present work the different phases have been formed at the same temperature and therefore it seems conclusive that the T_m of the β phase is higher than that of the α phase, and that the T_m of the γ phase is higher than the one of α and β phases. This order could be ascribed by relating the intensity of the melting peaks to the β and γ phase contents determined by FTIR. This would explain the result of exothermic crystallization peaks in the cooling scans shown in Fig. 3.

It is interesting to see in Fig. 9 (Hoffman-weeks extrapolation method) that those β phase melting temperatures move faster with the crystallization temperature than those of the α phase, which in the literature have been associated with the fact that the equilibrium melting temperature of these phases is higher than that of the α phase [5]. This is because the extrapolations of the line obtained at the melting temperature as a function of the isothermal temperature diagram (dashed lines in orange and grey, respectively, in Fig. 9) cut the line T_m=T_{iso} at higher values.

The intensity of the β phase melting drops rapidly from 154 °C and it

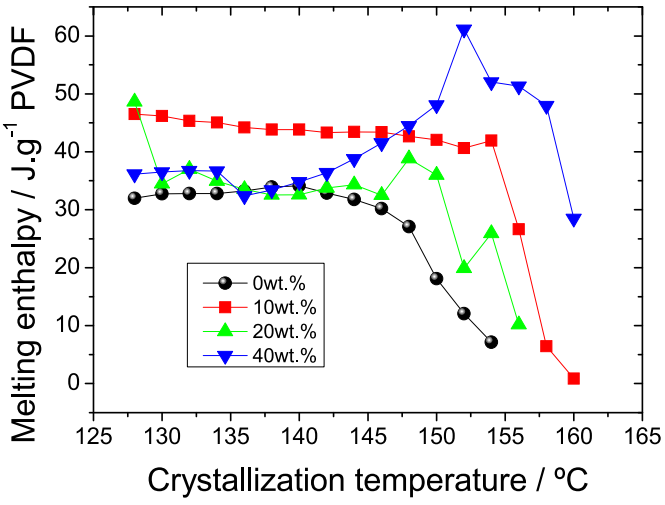

Fig. 10. Melting enthalpy of neat PVDF and PVDF blends with 10, 20 and 40 wt % of $[Emim]_2$ $[Co(SCN)_4]$ IL content crystallized at different temperatures.

is negligible from 158 °C on, both in the sample with 10 wt% and 20 wt % of IL content. The highest temperature melting peak is associated with the γ phase in mixtures with 10 and 20 wt% IL content, where the last T_c for which melting peaks can be observed is 158 °C, while in the mixture with 40 wt% of IL content, in which only a very wide melting peak is visible, even at 160 °C a very significant fraction of PVDF crystallizes.

The evolution of melting enthalpies for the various samples is represented in Fig. 10. Firstly, it is observed that melting enthalpy values increase with increasing IL content. On the other hand, values are

constant until approximately 154 °C, after which they drop very suddenly, while the neat PVDF sample has a much gradual and early drop, around 140 °C. These findings are in agreement with the previous analysis. Since the IL is a strong promoter of EA phase crystallization, it makes sense that these structures would need higher energy to melt, as it was also observed in Fig. 8. In the same way, this could also explain the early drop of the 0 wt% sample. Since the IL strongly induces β and γ structures, these melt at higher temperatures, prolonging the flatness of the graph, by being mainly absent in the neat PVDF sample. After the melting of α structures, which melt at lower temperatures, there are no structures to melt, hence no energy is absorbed by the sample and the enthalpy values drop. These data add up and further strengthen the conclusion that the presence of the IL has a strong inductor effect of electroactive phase crystallization of PVDF.

4. Conclusions

PVDF blends with the magnetic ionic liquid $[Emim]_2$ $[Co(SCN)_4]$ have been prepared for different ionic liquid content and the effect of the presence and content of the ionic liquid in polymer phase crystallization analyzed.

The presence of $[Emim]_2$ $[Co(SCN)_4]$ enhances the nucleation of PVDF in the electroactive phases, but at any crystallization temperature between 128 and 160 °C, a certain fraction of α crystals is also formed. The addition of $[Emim]_2$ $[Co(SCN)_4]$, then, has been shown to be a simple and very effective way to help maximize PVDF's electroactive phases and, since it is in liquid state, it can be easily removed when needed. Moreover, this induction of electroactive phases is dose dependent, as higher percentage of $[Emim]_2$ $[Co(SCN)_4]$ correlates to higher percentage of electroactive β and γ structures.

FESEM images of the samples containing 10 and 20 wt% of $[Emim]_2$ $[Co(SCN)_4]$ are very similar, but in the blend containing the 20 wt% of $[Emim]_2$ $[Co(SCN)_4]$, the images show how the IL is segregated.

The melting temperature of the γ phase is higher than that of the β phase and higher than that of the α phase for the same temperature of crystallization. This leads to an increase in the crystallization temperature observed in cooling scans with increasing e IL content, on the contrary to what one might expect due to the freezing point depression.

CRediT authorship contribution statement

Luis A. Martins: Writing – review & editing, Writing – original draft, Visualization, Validation, Investigation, Formal analysis. **José Luis Gómez Ribelles:** Writing – review & editing, Writing – original draft, Visualization, Validation, Project administration, Investigation, Funding acquisition, Formal analysis, Conceptualization. **Carlos M. Costa:** Writing – review & editing, Writing – original draft, Visualization, Supervision, Project administration, Investigation, Formal analysis, Conceptualization. **Daniela M. Correia:** Writing – review & editing, Writing – original draft, Visualization, Methodology, Investigation, Formal analysis. **Senentxu Lanceros-Méndez:** Writing – review & editing, Writing – original draft, Project administration, Investigation, Funding acquisition, Conceptualization. **Ivan Krakowsky:** Writing – review & editing, Writing – original draft, Validation, Investigation, Formal analysis. **Isabel Tort-Ausina:** Writing – review & editing, Writing – original draft, Visualization, Supervision, Investigation, Formal analysis, Conceptualization.

Declaration of competing interest

The authors declare that they have no known competing financial interests or personal relationships that could have appeared to influence the work reported in this paper.

Data availability

Data will be made available on request.

Acknowledgements

The authors thank the Fundação para a Ciência e Tecnologia (FCT) for financial Support under the framework of Strategic Funding UID/FIS/04650/2020, and UID/QUI/0686/2020 and under projects 10.54499/2022.03931. PTDC, 2022.05932. PTDC and POCI-01-0247-FEDER-046985 funded by national funds through FCT and by the ERDF through the COMPETE2020—Programa Operacional Competitividade e Internacionalização (POCI). The authors also thank the FCT for financial support under FCT investigator contracts 2020.02915. CEECIND (D.M.C), and 10.54499/2020.04028. CEECIND/CP1600/CT0018 (C.M.C.). The authors thank the Basque Government Education and Industry departments for funding under the IKUR and Elkartek programs, respectively. The work of the Spanish group has been funded by the Universitat Politècnica de València though the "Aid to First Research Projects (PAID-06-22), Vice-rectorate of Research of the Universitat Politècnica de València (UPV)", and by the Generalitat Valenciana (GVA) through a grant for stays of Doctorate academic and research staff in research centers located outside the Valencian Community convened by Resolution of October 6, 2022, of the Conselleria de Innovación, Universidades, Ciencia y Sociedad Digital (DOGV núm. 9449/September 14, 2021). This research was supported by CIBER -Consorcio Centro de Investigación Biomédica en Red- (CB06/01/1026), Instituto de Salud Carlos III, Ministerio de Ciencia e Innovación. The Microscopy Service of the Universitat Politècnica de València is gratefully acknowledged for helping with FESEM characterization.

Appendix A. Supplementary data

Supplementary data to this article can be found online at https://doi.org/10.1016/j.polymer.2024.126816.

References

[1] S. Bahl, H. Nagar, I. Singh, S. Sehgal, Smart materials types, properties and applications: a review, Mater. Today: Proc. 28 (2020) 1302–1306.
[2] C.M. Costa, V.F. Cardoso, P. Martins, D.M. Correia, R. Gonçalves, P. Costa, V. Correia, C. Ribeiro, M.M. Fernandes, P.M. Martins, S. Lanceros-Méndez, Smart and multifunctional materials based on electroactive poly(vinylidene fluoride): recent advances and opportunities in sensors, actuators, energy, environmental, and biomedical applications, Chem. Rev. 123 (19) (2023) 11392–11487.
[3] R. Dallaev, T. Pisarenko, D. Sobola, F. Orudzhev, S. Ramazanov, T. Trčka, Brief Review of PVDF Properties and Applications Potential 14 (22) (2022) 4793.
[4] S. Houis, E.M. Engelhardt, F. Wurm, T. Gries, Application of polyvinylidene fluoride (PVDF) as a biomaterial in medical textiles, in: S.C. Anand, J.F. Kennedy, M. Miraftab, S. Rajendran (Eds.), Medical and Healthcare Textiles, Woodhead Publishing2010, pp. 342-352..
[5] P. Martins, A.C. Lopes, S. Lanceros-Mendez, Electroactive phases of poly (vinylidene fluoride): determination, processing and applications, Prog. Polym. Sci. 39 (4) (2014) 683–706.
[6] C. Xing, M. Zhao, L. Zhao, J. You, X. Cao, Y. Li, Ionic liquid modified poly (vinylidene fluoride): crystalline structures, miscibility, and physical properties, Polym. Chem. 4 (24) (2013) 5726–5734.
[7] S.J. Kazmi, M. Nadeem, M.A. Warsi, S. Manzoor, B. Shabbir, S. Hussain, PVDF/CFO-anchored CNTs ternary composite system with enhanced EMI shielding and EMW absorption properties, J. Alloys Compd. 903 (2022) 163938.
[8] L.A. Martins, J. Ródenas-Rochina, D. Salazar, V.F. Cardoso, J.L. Gómez Ribelles, S. Lanceros-Mendez, Microfluidic processing of piezoelectric and magnetic responsive electroactive microspheres, ACS Appl. Polym. Mater. 4 (8) (2022) 5368–5379.
[9] R. Gonçalves, P. Martins, D.M. Correia, V. Sencadas, J.L. Vilas, L.M. León, G. Botelho, S. Lanceros-Méndez, Development of magnetoelectric CoFe2O4/poly (vinylidene fluoride) microspheres, RSC Adv. 5 (45) (2015) 35852–35857.
[10] Z.-W. Ouyang, E.-C. Chen, T.-M. Wu, Enhanced piezoelectric and mechanical properties of electroactive polyvinylidene fluoride/iron oxide composites, Mater. Chem. Phys. 149–150 (2015) 172–178.
[11] B. Pedroso Silva Santos, J.J. Rubio Arias, F.E. Jorge, R. Értola Pereira de Deus Santos, B. da Silva Fernandez, L. da Silva Candido, A.C. de Carvalho Peres, ÉGervasoni Chaves, M.d.F. Vieira Marques, Nanocomposites of poly(vinylidene

fluoride) with oxide nanoparticles for barrier layers of flexible pipes, J. Mater. Res. Technol. 15 (2021) 3547–3557.
[12] P. Li, W. Jiang, R. Lu, D. Yuan, J. Shan, J. Xiao, Design and durability of PZT/PVDF composites based on pavement perception, Construct. Build. Mater. 323 (2022) 126621.
[13] C. Zhang, H. Sun, Q. Zhu, Preparation and property enhancement of poly (vinylidene fluoride) (PVDF)/Lead zirconate titanate (PZT) composite piezoelectric films, J. Electron. Mater. 50 (11) (2021) 6426–6437.
[14] D.M. Correia, L.C. Fernandes, P.M. Martins, C. García-Astrain, C.M. Costa, J. Reguera, S. Lanceros-Méndez, Ionic liquid–polymer composites, A New Platform for Multifunctional Applications 30 (24) (2020) 1909736.
[15] R.M. Meira, D.M. Correia, A. García Díez, S. Lanceros-Mendez, C. Ribeiro, Ionic liquid-based electroactive materials: a novel approach for cardiac tissue engineering strategies, J. Mater. Chem. B 10 (34) (2022) 6472–6482.
[16] C. Bodin, B. Gelinas, J. Deng, K. Pithaksinsakul, Y. Zhu, D. Rochefort, O. Fontaine, Describing the unsuspected advantage of redox ionic liquids applied to electrochemical energy storage, Curr. Opin. Colloid Interface Sci. 64 (2023) 101677.
[17] K. Sirengo, A. Babu, B. Brennan, S.C. Pillai, Ionic liquid electrolytes for sodium-ion batteries to control thermal runaway, J. Energy Chem. 81 (2023) 321–338.
[18] T. Welton, Ionic liquids: a brief history, Biophys Rev 10 (3) (2018) 691–706.
[19] X. Wang, X. Li, J. Yue, Y. Cheng, K. Xu, Q. Wang, F. Fan, Z. Wang, Z. Cui, Fabrication of poly(vinylidene fluoride) membrane via thermally induced phase separation using ionic liquid as green diluent, Chin. J. Chem. Eng. 28 (5) (2020) 1415–1423.
[20] J.C. Barbosa, D.M. Correia, R. Gonçalves, V. de Zea Bermudez, M.M. Silva, S. Lanceros-Mendez, C.M. Costa, Enhanced ionic conductivity in poly(vinylidene fluoride) electrospun separator membranes blended with different ionic liquids for lithium ion batteries, J. Colloid Interface Sci. 582 (2021) 376–386.
[21] D.M. Correia, C.M. Costa, J.C. Rodríguez Hernández, I. Tort-Ausina, L.T. Biosca, C. Torregrosa Cabanilles, J. Meseguer-Dueñas, I. Krakovsky, S. Lanceros-Méndez, J. L. Gómez Ribelles, Crystallization monitoring of semicrystalline poly(vinylidene fluoride)/1-Ethyl-3-methylimidazolium hexafluorophosphate [emim][PF6] ionic liquid blends, Cryst. Growth Des. 21 (8) (2021) 4406–4416.
[22] D.M. Correia, C.M. Costa, E. Lizundia, R. Sabater i Serra, J.A. Gómez-Tejedor, L. T. Biosca, J.M. Meseguer-Dueñas, J.L. Gomez Ribelles, S. Lanceros-Méndez, Influence of cation and anion type on the formation of the electroactive β-phase and thermal and dynamic mechanical properties of poly(vinylidene fluoride)/ionic liquids blends, J. Phys. Chem. C 123 (45) (2019) 27917–27926.
[23] N. Subasree, J.A. Selvi, Imidazolium based ionic liquid derivatives; synthesis and evaluation of inhibitory effect on mild steel corrosion in hydrochloric acid solution, Heliyon 6 (2) (2020) e03498.
[24] J.P. Serra, L.C. Fernandes, N. Pereira, A. Fidalgo-Marijuan, J.M. Porro, C.M. Costa, D.M. Correia, S. Lanceros-Mendez, Humidity sensors based on magnetic ionic liquids blended in poly(vinylidene fluoride-co-hexafluoropropylene), ACS Appl. Polym. Mater. 5 (1) (2023) 109–119.
[25] T. Chatzimitakos, P. Anagnostou, I. Constantinou, K. Dakidi, C. Stalikas, Magnetic ionic liquids in sample preparation: recent advances and future trends, Separations 8 (9) (2021) 153.
[26] C. Ribeiro, C.M. Costa, D.M. Correia, J. Nunes-Pereira, J. Oliveira, P. Martins, R. Gonçalves, V.F. Cardoso, S. Lanceros-Méndez, Electroactive poly(vinylidene fluoride)-based structures for advanced applications, Nat. Protoc. 13 (4) (2018) 681–704.
[27] M. Avrami, Kinetics of phase change. I general theory, J. Chem. Phys. 7 (12) (2004) 1103–1112.
[28] M. Avrami, Kinetics of phase change. II transformation-time relations for random distribution of nuclei, J. Chem. Phys. 8 (2) (2004) 212–224.
[29] M. Avrami, Granulation, phase change, and microstructure kinetics of phase change. III, J. Chem. Phys. 9 (2) (2004) 177–184.
[30] L. Ruan, X. Yao, Y. Chang, L. Zhou, G. Qin, X. Zhang, Properties and applications of the β phase poly(vinylidene fluoride), Polymers (2018) 228.
[31] J. Gregorio, Rinaldo, M. Cestari, Effect of crystallization temperature on the crystalline phase content and morphology of poly(vinylidene fluoride), J. Polym. Sci. B Polym. Phys. 32 (5) (1994) 859–870.
[32] D.M. Correia, R. Goncalves, C. Ribeiro, V. Sencadas, G. Botelho, J.L. Gomez-Ribelles, S. Lanceros-Mendez, Electrosprayed poly(vinylidene fluoride) microparticles for tissue engineering applications, RSC Adv. (2014) 33013–33021.
[33] X. Cai, T. Lei, D. Sun, L. Lin, A critical analysis of the α, β and γ phases in poly (vinylidene fluoride) using FTIR, RSC Adv. (2017) 15382–15389.
[34] V.B.F. Mathot, Calorimetry and Thermal Analysis of Polymers, Hanser1994..
[35] G.R. Strobl, The Physics of Polymers : Concepts for Understanding Their Structures and Behavior, 2nd. corrected ed., Springer, 1997.
[36] V. Sencadas, R. Gregorio, S. Lanceros-Méndez, α to β phase transformation and microestructural changes of PVDF films induced by uniaxial stretch, J. Macromol. Sci., Part B 48 (3) (2009) 514–525.
[37] M. Sharma, G. Madras, S. Bose, Process induced electroactive β-polymorph in PVDF: effect on dielectric and ferroelectric properties, Phys. Chem. Chem. Phys. 16 (28) (2014) 14792–14799.
[38] P. Martins, C.M. Costa, M. Benelmekki, G. Botelho, S. Lanceros-Mendez, On the origin of the electroactive poly(vinylidene fluoride) β-phase nucleation by ferrite nanoparticles via surface electrostatic interactions, CrystEngComm 14 (8) (2012) 2807–2811.
[39] G.-d. Kang, Y.-m. Cao, Application and modification of poly(vinylidene fluoride) (PVDF) membranes – a review, J. Membr. Sci. 463 (2014) 145–165.
[40] C.M. Costa, V.F. Cardoso, R. Brito-Pereira, P. Martins, D.M. Correia, V. Correia, C. Ribeiro, P.M. Martins, S. Lanceros-Méndez, Chapter 1 - electroactive poly (vinylidene fluoride)-based materials: recent progress, challenges, and opportunities, in: B. Ameduri, S. Fomin (Eds.), Fascinating Fluoropolymers and Their Applications, Elsevier2020, pp. 1-43..
[41] R. Gonçalves, P.M. Martins, C. Caparrós, P. Martins, M. Benelmekki, G. Botelho, S. Lanceros-Mendez, A. Lasheras, J. Gutiérrez, J.M. Barandiarán, Nucleation of the electroactive β-phase, dielectric and magnetic response of poly(vinylidene fluoride) composites with Fe2O3 nanoparticles, J. Non-Cryst. Solids 361 (2013) 93–99.
[42] S. Mishra, R. Sahoo, L. Unnikrishnan, A. Ramadoss, S. Mohanty, S.K. Nayak, Investigation of the electroactive phase content and dielectric behaviour of mechanically stretched PVDF-GO and PVDF-rGO composites, Mater. Res. Bull. 124 (2020) 110732.
[43] M.N. Tamaño-Machiavello, C.M. Costa, F.J. Romero-Colomer, J. María Meseguer Dueñas, S. Lanceros-Mendez, J. Luis Gómez Ribelles, Crystallization kinetics of poly(ethylene oxide) confined in semicrystalline poly(vinylidene) fluoride, J. Polym. Sci. B Polym. Phys. 56 (7) (2018) 588–597.
[44] R. Gregorio, R.C. CapitãO, Morphology and phase transition of high melt temperature crystallized poly(vinylidene fluoride), J. Mater. Sci. 35 (2) (2000) 299–306.